Renewable Energy 177 (2021) 1282–1292

Contents lists available at ScienceDirect

Renewable Energy

journal homepage: www.elsevier.com/locate/renene

Pyrolysis behaviour, kinetics and thermodynamic data of hydrothermal carbonization–Treated pulp and paper mill sludge

Shule Wang [a, *, 1], Yuming Wen [a, 1], Henry Hammarström [a, b], Pär Göran Jönsson [a], Weihong Yang [a]

[a] KTH Royal Institute of Technology, School of Industrial Engineering and Management, Department of Materials Science and Engineering, Brinellvägen 23, 114 28, Stockholm, Sweden
[b] RISE - Research Institutes of Sweden, Box 5604, SE-114 86, Stockholm, Sweden

ARTICLE INFO

Article history:
Received 8 January 2021
Received in revised form
18 May 2021
Accepted 4 June 2021
Available online 12 June 2021

Keywords:
HTC
Pyrolysis
Paper sludge
Kinetics

ABSTRACT

Organic-rich pulp and paper mill sludge (PPMS) has the potential to become a renewable carbon source for producing alternatives to fossil-based product. In this work, PPMS treated by hydrothermal carbonization (HTC) was investigated based on its pyrolysis properties. The pyrolytic mechanism, kinetics data and product of the sample were studied using TG as well as pyrolysis tests in Py-GC/MS and a bench-scale reactor at 450, 550, and 650 °C. The results show that the thermal decomposition of feedstock is a two-stage reaction. The mean activation energy of the pyrolysis of HTC treated PPMS was estimated as 233.08 kJ/mol, which is higher than that of the pyrolysis of paper sludge reported before. The changes in enthalpies, entropies and Gibbs free energies from the reactants to the activated complex were estimated. The concentration of monocyclic aromatic hydrocarbons in the derived organic liquid fraction shows a positive correlation with the pyrolysis temperature. At 550 °C, the organic liquid fraction reached its highest yield at 13.7% with an oxygen level of 10.7 wt% and a higher heating value of 35.9 MJ/kg. The pyrolytic chars show that a molar ratio of O:C is less than 0.2, which shows potential for use as a carbon sink.

1. Introduction

Pulp and paper mill sludge (PPMS) is a solid residue derived from the sedimentation step during the wastewater treatment process in the pulp and paper industries. PPMS contains wood fibres and chemical contaminants [1]. The annual production of PPMS is approximately four hundred million tons globally [2]. In addition, around 695.7 million m^3 of wastewater was produced from pulp and paper mill industries worldwide per year [3]. The conventional management of PPMSs includes landfilling and energy recovery by using combustion. However, the land application of PPMS is limited due to the resulting environmental problems, such as emission of hazardous organic compounds and greenhouse gases, pollution and eutrophication of groundwater, and heavy metal contamination of the environment [4]. Therefore, research on sustainable recycling methods of PPMSs is of interest.

Pyrolysis is a technology which allows producing of char, liquid and gas from biomass materials. The char product has the potential to be used as absorbent, carbon sink and solid fuel [5–7]. The liquid product derived from biomass through pyrolysis has been recognized as a) feasible alternative to liquid fossil fuel [8]; b) sustainable source for chemical production [9]. The application of gas product as feedstock for methanation or steam reforming process is widely studied [10,11]. The abundant wood fibres make PPMS a potential biomass resource for pyrolysis process. However, the high moisture content of PPMS (70–80 wt% moisture content after mechanical dewatering) increases the cost of the transportation and drying process [12]. The high moisture content of sludge also provides microorganisms with a suitable environment to digest the organics in sludge, which would result in the emission of greenhouse gases. Therefore, a pretreatment, which can decrease the moisture content of PPMS and stabilize PPMS, would enhance the value of PPMS as a potential resource to, for example produce liquid biofuels. Hydrothermal carbonization (HTC) is a known process for producing hydrochar from biomass. In HTC, a wet feedstock is heated to approximately 180–220 °C under pressures of 20–25 bars in a high-pressure vessel [13]. The HTC process results in the

* Corresponding author. Brinellvägen 23, Stockholm, SE-114 28, Sweden.
E-mail address: Shule@kth.se (S. Wang).
[1] These authors contributed equally to this work.

https://doi.org/10.1016/j.renene.2021.06.027

dissolution of hydrophilic components of the feedstock and the formation of a hydrophobic solid residue with enhanced dewaterability [13]. Compared to the conventional thermal drying process, HTC pretreatment followed by mechanical dewatering has been proven to result in a 70% reduction in the energy consumption of sludge drying [12]. In addition, the hydrochar produced from HTC treatment has a lower O:C ratio than that of the raw material, which is more desirable when it is used as a feedstock for pyrolysis [14]. Pyrolysis is one of the most promising thermochemical conversion technologies to produce bio-oil from biomass. During the pyrolysis process, biomass is heated in an inert atmosphere, which causes decomposition of the polymeric structure of biomass. Three phases of products, solid, liquid, and gas, would be produced. The solid product can be applied as a soil amendment, carbon sink, and activated carbon. The liquid product can be further enhanced and extracted to produce liquid fuels or chemicals. The gas product, which includes a high concentration of CO, H_2, and CH_4 gases, can be used for energy applications. Therefore, a process that combines the HTC and pyrolysis processes could contribute to the production of several fractionated and valorized products from PPMS and to overall enhance the value of products derived from PPMS.

Pyrolysis studies via thermogravimetric analysis (TGA) can guide the design and optimization of the process [15]. Based on the TG results, model-free methods, such as the Kissinger-Akahira-Sunose (KAS), Ozawa-Flynn-Wall (OFW), and Friedman methods, can be applied to estimate kinetic parameters such as activation energy (E_a) and pre-exponential factor (A) [16]. The thermodynamic parameters of the conversion from reactants to the activated complex, such as enthalpy $\Delta H^{\ddagger}$, Gibbs free energy $\Delta G^{\ddagger}$ and entropy $\Delta S^{\ddagger}$, can be estimated by combining the Arrhenius equation and transition state theory [17]. The combination of kinetic and thermodynamic parameters is an essential factor for designing and optimizing pilot-scale industrialization [18]. Pyrolysis-gas chromatography/mass spectrometry (Py-GC/MS) is a method that is applied to the evaluation of the composition of pyrolytic volatiles [19–21]. Py-GC/MS allows for efficient research on the changes in the pyrolytic vapour product depending on the changes in pyrolysis conditions. The bench-scale reactor allows the estimation of product yields and can be performed on various scale, gram-to kilogram-scale pyrolytic products, which allows the determination of the mass and energy balance analysis of pyrolysis products. Moreover, the ultimate and proximate analysis of bench-scale pyrolytic products can further contribute to discovering the potential application of such pyrolytic products.

The objectives of this work were to evaluate the pyrolysis behaviour and kinetics of HPPMS. In this study, PPMS was first treated via HTC (HPPMS). The HPPMS was studied by using TG, Py-GC/MS, and a bench-scale reactor. The thermodynamic and kinetic parameters of HPPMS pyrolysis were estimated. The evaluation of components in the pyrolytic vapour was studied. The mass and energy balance and characterization of the pyrolytic products were investigated.

2. Materials and methods

2.1. Feedstock materials and HTC treatment

The PPMS was treated via HTC in C-Green's continuous HTC pilot plant in Örnsköldsvik, Sweden. The HTC treatment was performed at 200 °C with a solid residence time of 1 h. The dry solid (DS) concentration is 15 wt% in the PPMS. No additional water was added into the HTC reactor. The solid yield was 55 wt% of dry solid after HTC. The resulting solid product HPPMS was ground and sieved to a particle size of <0.5 mm, followed by drying at 105 °C for 24 h prior to pyrolysis experiments. The temperature of HTC was chosen according to the study by Ying et al. [22]. When the temperature of HTC increased above 200 °C, the cellulose in the solid product started to break down into soluble organics and permanent gas [23], which resulted in a lower product yield in the following pyrolysis process.

2.2. Thermogravimetric analysis

The thermal decomposition of HPPMS were studied on a laboratory thermogravimetric analyser (STA 449 F1 Jupiter, Netzsch) at atmospheric pressure. In each experiment, 5 mg of HPPMS sample was placed in an Al_2O_3 ceramic crucible in an N_2 atmosphere, heated from 25 to 120 °C, and held at a constant temperature for 5 min for sample drying. Then, the sample was heated from 120 to 900 °C with a heating rate of 10/15/20 °C/min followed by a constant temperature of 900 °C for 10 min. The TG results derived from the temperature range of 120–900 °C were further studied based on differential thermogravimetry (DTG) analysis.

2.2.1. Kinetic analysis using model-free methods

The kinetic analysis is conducted using model-free methods based on the TGA and DTG results of HPPMS. The basic kinetic equation can describe the pyrolysis of HPPMS:

$$\frac{d\alpha}{dt} = K(T)f(\alpha) \tag{1}$$

where α is the normalized conversion of the decomposition of raw materials:

$$\alpha = \frac{m_0 - m_t}{m_0 - m_f} \tag{2}$$

where m_0 is the initial mass (mg), m_t is the mass at given time t (mg), m_f is the final mass of the sample (mg), and $f(\alpha)$ is a function that depends on the mechanism of the reaction.

According to the Arrhenius equation, the temperature-dependent function $K(T)$ can be described as:

$$K(T) = Aexp\left(-\frac{E_a}{RT}\right) \tag{3}$$

where A is the pre-exponential factor (min^{-1}), E_a is the activation energy (J/mol), and R is the global gas constant (8.3145 J/(mol K)).

In the TG experiment with a constant heating rate β, the temperature T can be described as:

$$T = T_0 + \beta\, t \tag{4}$$

where T_0 is the original temperature, β is the heating rate, and t is the reaction time.

Differentiating the above correlation

$$dT = \beta\, dt \tag{5}$$

By integrating equation (3), the integral form of the reaction model is derived:

$$g(\alpha) = \int_0^{\alpha} \frac{d\alpha}{f(\alpha)} = \frac{A}{\beta} \int_{T_0}^{T_{max}} exp\left(-\frac{E_a}{RT}\right) dT \tag{6}$$

It is impossible to obtain the analytical solution of the right side of equation (6). Thus, some approximation methods have been applied to estimate the related kinetics values [24]. The model-free method is also known as the isoconversional method because its

reaction rate is defined as a function of temperature at constant conversion [25]. Model-free methods can evaluate the kinetic parameters of the Arrhenius equation without assuming the kinetic model of the reaction. In all model-free methods, data from several measurements with different heating rates are needed. The activation energy E_a at each conversion was determined according to different methods [26]. In this work, three isoconversional methods, KAS, OFW, and Friedman, are used to evaluate the kinetic parameters of the pyrolysis of HPPMS.

The KAS method is a commonly used integral isoconversional method that describes the correlation between the temperature and heating rate [27]. The KAS equation can be defined as the following:

$$ln\left(\frac{\beta}{T^2}\right)|_\alpha = ln\left(\frac{AR}{E_a g(\alpha)}\right) - \frac{E_a}{RT} \quad (7)$$

By plotting $ln(\beta/T^2)$ against $1/T$, the activation energy E_a could then be determined from the slope rate [28].

The OFW method is an integral isoconversional method that applies Doyle's approximation [27] to estimate the kinetic parameters. The equation of OFW method:

$$ln(\beta)|_\alpha = ln\left(\frac{AE_a}{Rg(\alpha)}\right) - 5.331 - 1.052\frac{E_a}{RT} \quad (8)$$

Similar to the KAS method, the activation energy E_a can be obtained as the slope $-1.052E_a/R$ [29,30].

The Friedman method is a differential isoconversional method that assumes that the reaction function $f(\alpha)$ only depends on the mass loss rate [31]. The FR equation can be written as follows:

$$ln\left(\frac{d\alpha}{dt}\right) = lnf(\alpha) + lnA - \frac{E_a}{RT} \quad (9)$$

By evaluating the slope of $ln(d\alpha/dt)$ versus $1/T$, the activation energy E_a can be calculated.

In this work, kinetic analysis software (NETZSCH Kinetics Neo) was applied to analyze the kinetic parameters using model-free methods.

2.2.2. Calculation of thermodynamic parameters

The thermodynamic parameters of the reactions in which the initial reactants transfer to the activated complex, such as changes in enthalpy ($\Delta H^{\ddagger}$, kJ/mol), Gibbs free energy ($\Delta G^{\ddagger}$, kJ/mol), and entropy ($\Delta S^{\ddagger}$, kJ/mol. K) can be calculated based on the kinetic data using the following equations [32]:

$$\Delta H^{?} = E_a - RT \quad (10)$$

$$\Delta G^{?} = E_a + RT_m ln\left(\frac{K_B T_m}{hA}\right) \quad (11)$$

$$\Delta S^{\ddagger} = \frac{\Delta H^{\ddagger} - \Delta G^{\ddagger}}{T_m} \quad (12)$$

where T_m is the DTG peak temperature (K), K_B is the Boltzmann constant (1.381×10^{-23} J/K), and h is the Plank constant (6.626×10^{-34} Js).

In this study, thermodynamic parameters, including changes in enthalpy, Gibbs free energy, and entropy from reactants to the activated complex in the HPPMS pyrolysis process, are estimated from the results of model-based kinetic analysis.

2.3. Micro-scale pyrolysis test

The pyrolysis experiment of HPPMS was performed with a Py-GC/MS system consisting of a Pyrola2000 (Pyrol AB, Sweden) combined with an Agilent 7890A GC coupled with an Agilent 5975C MS. A VF-1701MS column was used in the GC. For each test, a 1 mg sample was pyrolyzed in the Pyrola2000 unit. Pyrolysis tests were performed at temperatures of 450, 550, and 650 °C. After pyrolytic vapour was injected into the GC column, the GC oven was kept at 40 °C for 2 min. Then, the oven was heated to a temperature of 250 °C at a rate of 4 °C/min. After that, the temperature was kept at 250 °C for 50 min. Compounds with molar masses ranging from 46.0 to 256.4 g/mol were studied. Based on the derived chromatogram and analysis in ChemStation using the NIST11 library, the peaks were identified and integrated. The identified compounds were classified into compound groups. Then, the abundance of each compound group is represented as a peak area percentage value.

2.4. Bench-scale pyrolysis experiments

2.4.1. Experimental procedure and fixed bed reactor

Experiments at 450, 550, and 650 °C were performed in a fixed bed reactor to evaluate the pyrolytic product distribution and liquid quality derived at different temperatures. The fixed bed reactor illustrated in Fig. A1 in the supplementary file, which included a vertical steel tube with an inner diameter of 5 cm, an electrical heating furnace 60 cm in length, and a water-cooled zone 20 cm at the top of the system. The system is further described in previous works [8,33–35]. Before each experiment, HPPMS was dried in a conventional drying oven at 105 °C for 24 h. For each experiment, 50 g of HPPMS sample was placed in a stainless-steel crucible and positioned in the water-cooled zone above the furnace. The sample was introduced into the furnace when the furnace had reached the set temperature. The carrier gas employed in this study was nitrogen, which was set at a constant room-temperature flow rate of 100 ml/min. The liquid product was condensed in washing bottles placed in a cooling bath operated at −20 °C. Then, the permanent gas was collected in a gas sampling bag for further analysis.

2.4.2. Gas analysis

Gas analysis was performed with Agilent 490 micro-GC gas chromatography (GC) equipment. The micro-GC was calibrated with respect to the following elements: CH_4, C_2H_2, C_2H_4, C_2H_6, C_3H_6, C_3H_8, CO, CO_2, H_2, H_2S, N_2, and O_2. Then, the heating value was calculated based on the gas composition and the derived gas volume [36].

2.4.3. Liquid analysis

Liquid products derived from the bench-scale experiments were separated into organic and aqueous fractions in a funnel by gravity. Elemental analysis of the liquid products was performed at the Institute of Chemical Industry of Forest Product CAF (Nanjing, China). The higher heating value of the organic fraction was estimated by using Dulong's equation (equation (13)) [37]. The water content of the aqueous fraction was determined using Karl Fischer titration with standard method ASTM E203 [38].

$$HHV\left[MJ/kg\right] = 33.930m_c + 144.320\left(m_H - m_O/8\right) + 9.300m_S + 1.494m_N \quad (13)$$

where m_C, m_H, m_O, m_S, and m_N are the weight percentages of carbon, hydrogen, oxygen, sulfur, and nitrogen, respectively;

2.4.4. Feedstock and char analysis

Ultimate and proximate analyses of the char and HPPMS were performed with the standard methods listed in Table B1 in the supplementary file. The analysis data of PPMS is provided by the industrial partner of HTC process C-Green AB, Sweden.

Ash oxidation behaviour was found in the study of HCP of digested municipal sewage sludge [35]. This ash oxidation behavior resulted in difficulties in fixed carbon content determination of the char. A new method NOAC was proposed to analyze the fixed carbon and nonoxidized ash content of this type of pyrolytic char. The result of the ash oxidation behaviour of HPPMS is presented Appendix C in the supplementary file.

3. Results and discussion

3.1. Hydrothermal carbonization

The PPMS was treated in the HTC pilot plant owned by C-Green AB, followed by mechanical dewatering to achieve the final HPPMS. The ultimate and proximate analysis of mechanically dewatered PPMS (as received from a Swedish pulp and paper industry) and HPPMS is presented in Table 1. The metal composition of the HPPMS is included in the supplementary material in Table B2 Both the C:H and C:O ratios were increased by the pretreatment step. The water balance of the HTC process is given by C-Green AB presented in Table 2. It was claimed that it is hard to increase the DS content above 20% of PPMS by mechanical dewatering by C-Green. With the HTC treatment and a presser for dewatering, the DS content of HPPMS can be increased to 55% [39]. According to Table 2, after treated by HTC process followed by water pressing, 93.5% of water in the PPMS can be removed.

3.2. Thermogravimetric analysis

The thermal decomposition behaviour of HPPMS were investigated based on thermogravimetric analysis (TGA). The results from TGA and DTG are presented in Fig. 1. According to the DTG results, the thermal decomposition of HPPMS can be described as a two-stage reaction: the most significant DTG peak can be seen as the first stage and the rest is classified as the second one. The two stages are divided by the highest DTG values between the peaks of the DTG curve. The temperature ranges of the first stage differed with different heating rates, which are shown in Table 3. The mass loss during stage 1 ranged from 42.7 to 50.8% with various heating rates. The DTG peak at ~325 °C could be explained by the thermal decomposition of the cellulose fraction, while the shoulder at 400 °C represented the decomposition of lignin [40]. The overall result differed from the DTG study of woody biomass, which also included another peak mainly corresponding to the decomposition of hemicellulose at approximately 260 °C [40]. During the HTC treatment of lignocellulosic biomass, hemicellulose usually degrades below 200 °C, cellulose degrades at 200–230 °C, and lignin degrades from 220 to 260 °C [41]. The PPMS used in this study was treated in HTC at 200 °C, and the hemicellulose fraction could be removed during HTC treatment. During the second stage, the degradation observed in the TGA results, occurring after the end of stage 1–900 °C, showed that ~30 wt% of the sample was decomposed. Similar cases were observed in other TGA results derived from PPMS [42]. This peak could be partially attributed to the thermal decomposition of calcium carbonate in the intrinsic ash in the material. In a TG-FTIR analysis of PPMS performed by Li et al., CO_2 production was found in this temperature range of 600–900 °C, supporting the hypothesis of thermal decomposition of calcium carbonate [42].

3.3. Kinetic and thermodynamic studies

3.3.1. Kinetic analysis

Stage 1 of the pyrolysis reaction of HPPMS mainly corresponds to the thermal decomposition of organic matter. However, the exact initial temperature T_i, final temperature T_f, and temperature T_m where the DTG curves reach their peaks are different with various heating rates. The temperature range applied in this study for the kinetic study of the three different heating rate results as well as the T_m are shown in Table 3.

Three model-free methods were adopted to conduct the kinetic analysis of the first main mass loss stage of HPPMS pyrolysis. The model plots of the KAS, OFW, and Friedman methods within the same conversion range ($\alpha = 0.01, 0.02, \ldots, 0.99$) are shown in Fig. 2. It is obvious that the isoconversional lines are not parallel in all model plots, which indicates the change in evaluating kinetic parameters during the whole process [43]. Thus, more than one reaction occurs during the first main mass loss stage. The 1000/T range of ~1.6–~1.8 K^{-1} corresponds to the temperature range of ~282–~352 °C. This temperature region contains the highest densities of isoconversional lines of the three model plots. Moreover, these isoconversional lines in this range show a strong parallel relationship. According to previous studies, cellulose thermal decomposition typically occurs between 280 °C and 360 °C. Furthermore, the reaction rate reaches its peak at approximately 339–350 °C [16,44], which means that the reaction rate decreases when the temperature continuously increases after reaching ~350 °C. Thus, these results confirm that cellulose exists in HPPMS and contributes to the largest mass loss during pyrolysis of HPPMS.

The activation energy and pre-exponential factors at different conversion rates obtained by using the KAS, OFW, and FR methods are shown in Fig. A2 and Fig. A3 in the supplementary file, respectively. Compared to the FR method, the activation energies at each conversion rate deduced from the KAS and OFW methods are very similar. This is because the FR method is based on differential calculation, while both KAS and OFW are integral isoconversional

Table 1
Proximate and ultimate composition of the HPPMS used in the study.

Proximate analysis			Ultimate Analysis [wt%, db]		
	PPMS	HPPMS		PPMS	HPPMS
Moisture at 105 °C [wt%]	85.8–87.6	8.4	C	44.9–48.4	51.8
Ash content [wt%, db]	11.9–16.4	16.4	H	5.3–5.7	4.9
Volatile matter [wt%, db]	–	62.4	O	23.6–24.4	19.0
Fixed carbon [wt%, db]	–	21.2	N	5.5–7.9	4.2
HHV [MJ/kg, db]	–	21.5	Cl	0.0–0.1	0.029
			S	1.7–2.7	1.5

db: dry basis.

Table 2
The water balance in HTC process tonne water per tonne DS in sludge [39].

	Water in			Water out		
	Water in sludge (15% DS)	Sealing water	Water formed in process	Water in hydrochar (55% DS)	Water in off-gases	Water in filtrate return
Mass (tonne)	6.15	0.05	0.2	0.4	0.2	5.8

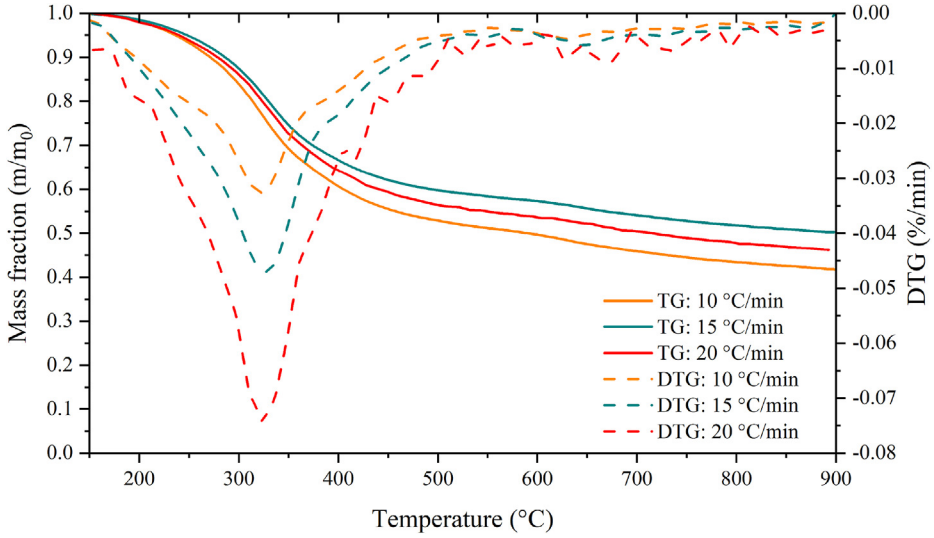

Fig. 1. TG and DTG results of pyrolysis of HPPMS with different heating rates.

Table 3
T_i and T_f defined in this study for the kinetic analysis of stage 1 of pyrolysis of HPPMS as well as the T_m in the ranges.

Heating rate (°C/min)	T_i (°C)	T_m (°C)	T_f (°C)
10	162	320	549
15	170	327	576
20	174	328	594

methods. The mean value of activation energies ($E_{a,\ mean}$) and the mean value of the logarithmic function of pre-exponential factors ($log(A)_{mean}$) deduced from the three model-free methods are given by Table 4. The mean values of the kinetic parameters estimated from the KAS and OFW methods are also close: the $E_{a,\ mean}$ values are 209.78 and 207.46 kJ/mol, while the $log(A)_{mean}$ values are 15.97 and 15.96 s^{-1}, respectively. On the other hand, $E_{a,\ mean}$ is 233.08 kJ/mol, and $log(A)_{mean}$ is 17.83 s^{-1} for the FR method. To compare the kinetic parameters of the pyrolysis of HPPMS to those of existing works, Table 4 also lists the kinetic parameters obtained from previous studies of the pyrolysis of paper sludge, hydrochar, and corn stover. In the study by Lin et al., the activation energy of the pyrolysis of paper sludge by using the Friedman method is 217 kJ/mol [45], which is slightly lower than the activation energy obtained in this work with the Friedman method. Ma et al. studied the kinetics of the pyrolysis of hydrochar produced from sawdust, and the activation energies were found to be 174.01 and 172.64 kJ/mol by using the KAS and OFW methods, respectively [46]. These results are ~35 kJ/mol lower than the data for HPPMS when using the same kinetic analysis method.

The conversion fitting results between the experimental data and the simulated curves deduced by the three model-free methods are shown in Fig. A4 in the supplementary file. The Friedman method simulating the curve of the conversion rate shows the best fitting performance with an R^2 equal to 0.9999, while the R^2 values of KAS and OFW are 0.9830 and 0.9840, respectively. It is known that the kinetic parameters yielded by using the Friedman method have better accuracy than those of the KAS and OFW methods [47].

3.3.2. Thermodynamic analysis

As shown in Table 3, T_i, T_f, and T_m changed when the heating rates were different. Therefore, using equations (10-12) to calculate the thermodynamic parameters can also yield different $\Delta H^{\ddagger}$, $\Delta G^{\ddagger}$, and $\Delta S^{\ddagger}$ with different heating rates. To solve this problem, it has been recommended that the thermodynamic parameters should be calculated based on the TG data obtained by using the lowest heating rate [51]. The lower the heating rate is, the more accurate the TG result will be [52]. Therefore, in this study, the thermodynamic parameters are estimated based on the TG results obtained from the 10 °C/min heating rate, and the results are shown in Fig. 3.

$\Delta H^{\ddagger}$ represents the heat absorbed or released during a reaction. All the obtained $\Delta H^{\ddagger}$ values are positive, which indicates that forming the activated complex from the reactants during the whole process of the pyrolysis of HPPMS results in endothermal conversions. For the $\Delta H^{\ddagger}$ of pyrolysis of HPPMS deduced from the Friedman methods, when the conversion degree is between 0.2 and 0.7, $\Delta H^{\ddagger}$ ranges from 264.00 to 315.60 kJ/mol; however, the conversion degree decreases sharply to 169.85 kJ/mol when the conversion degree reaches 0.8. A similar $\Delta H^{\ddagger}$ trend has been reported by Kaur et al. for the pyrolysis of castor [53]. It is known that the thermal decomposition of cellulose has a peak at ~355 °C [54]. The temperature is 398 °C when the conversion reaches 0.8, where the endothermic reaction of the pyrolysis of cellulose is nearly finished [55], which should be the main reason for the sharp decrease in $\Delta H^{\ddagger}$. On the other hand, for the $\Delta H^{\ddagger}$ evaluated by using the KAS and OFW methods, the $\Delta H^{\ddagger}$ at the same conversion degree are quite similar. The estimated $\Delta H^{\ddagger}$ ranges from 188.91 to 260.85 kJ/mol, which is obviously lower than the $\Delta H^{\ddagger}$ deduced by using the

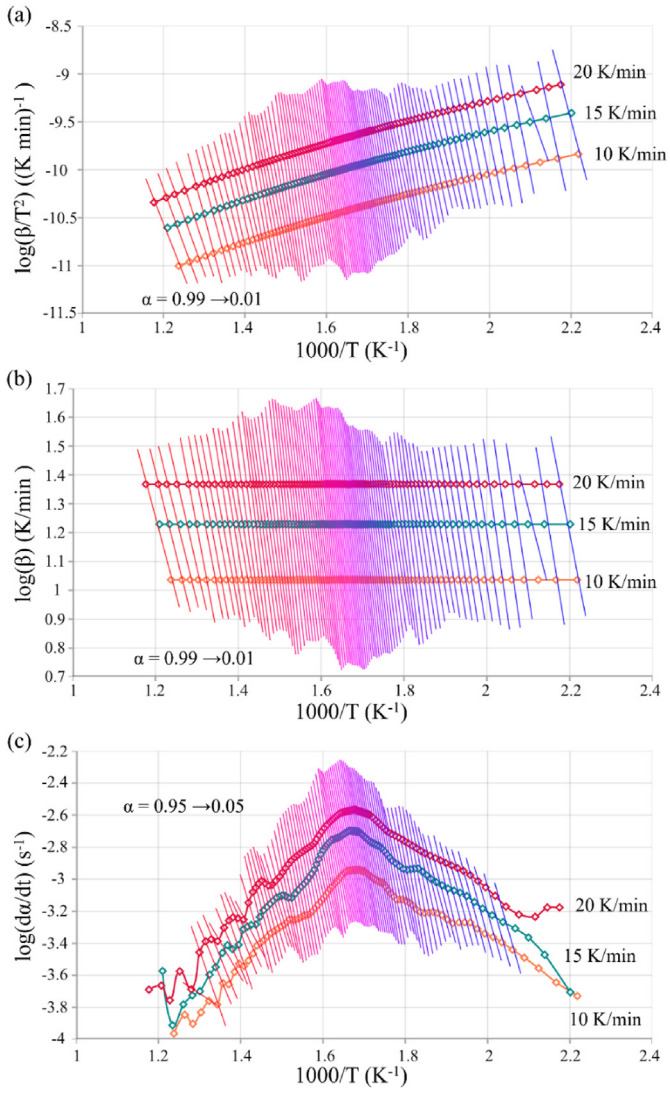

Fig. 2. Kinetic plots for pyrolysis of HPPMS using the (a) KAS, (b) OFW, and (c) Friedman methods.

Friedman method. From Table 4, it can be seen that the $\Delta H^{\ddagger}$ of the pyrolysis of HPPMS is between that of the $\Delta H^{\ddagger}$ of hydro-sawdust (168.09 kJ/mol) and hydro-sewage sludge (306.77 kJ/mol) [46].

$\Delta G^{\ddagger}$ is the total energy difference in the system before and after a reaction. The $\Delta G^{\ddagger}$ evaluated in this study varies from 158.89 to 198.87 kJ/mol. Moreover, $\Delta G^{\ddagger}$ has a proportional relationship to the conversion degree, as shown in Fig. 3. Therefore, the reaction of forming an activated complex for the pyrolysis of HPPMS is increasingly unfavourable when the conversion degree is increasing from 0.2 to 0.8. Thus, a higher temperature is needed to keep the reaction forward. The $\Delta G^{\ddagger}$ of the pyrolysis of HPPMS is very similar to that of hydro-sawdust, which is 168.09 kJ/mol [46].

$\Delta S^{\ddagger}$ can measure the changes in the disorder extent of a system. When the conversion degree is between 0.2 and 0.7, $\Delta S^{\ddagger}$ calculated based on the Friedman method varies from 109.81 to 235.78 J/mol. The K and $\Delta S^{\ddagger}$ values calculated based on the KAS and OFW methods range from 64.00 to 145.80 J/mol.K. A positive $\Delta S^{\ddagger}$ means that degree of disorder of the system increased from the reactants to the activated complex, which reveals that the reaction prefers to occur. Nevertheless, $\Delta S^{\ddagger}$ becomes negative when the conversion degree is 0.8. This probably corresponds to the end of the pyrolysis of cellulose: when a reaction is finished, the materials in the system are very near thermodynamic equilibrium. In this state, the materials in the system are inactive [53].

3.4. Micro-scale pyrolysis test

Py-GC/MS analysis of the HPPMS sample was performed at three temperatures: 450, 550, and 650 °C. The organic composition of pyrolytic vapour was identified and classified into different compound groups based on chemical characteristics. The area percentage of each compound group is presented in Fig. 4. The nitrogen-containing compound group refers to compounds that contain nitrogen, such as amines and amino acids, except for N-heterocyclics such as pyridines, pyrroles, and indoles. The appearance of these N-containing compounds reveals the existence of protein content in the feedstock. When the proteins and protein derivates degrade during pyrolysis, amine and amides are first generated; thereafter, additional N-heterocyclics are formed when the temperature is above 500 °C [56], which corresponds to this study. According to Fig. 4, the peak area percentage of aromatic hydrocarbons and phenols increased with increasing treatment temperature from 450 to 650 °C, i.e., a higher temperature resulted in a higher peak area percentage of aromatic hydrocarbons and phenols. Therefore, the selectivity towards aromatics was enhanced at higher temperatures, mainly because of the advanced decomposition of lignin with increasing temperature.

Sulfur-containing compounds were identified and are presented in Fig. A5 in the supplementary file. The selectivity of carbonyl sulfide and methanethiol was constant when the pyrolysis temperature was changed. However, there is no significant difference in the abundance of sulfur dioxide in pyrolytic vapour between 550 °C and 650 °C.

The peak area percentages of aromatic hydrocarbon compounds are presented in Fig. A6 in the supplementary file**.** The selectivity of all identified monocyclic aromatic hydrocarbons (MAHs) increased with treatment temperature. At the same time, the abundance of polyaromatic hydrocarbons (PAHs) decreased as the temperature increased. Aromatic hydrocarbons are promising alternatives to fossil fuel, which has a high heating value [57]. The overall results show that the organic fraction of pyrolytic vapour has a strong potential to be used as a high-energy liquid fuel.

3.5. Bench-scale pyrolysis experiments

3.5.1. Product distribution

The distribution of bench-scale pyrolysis products is presented in Table 5. At 550 °C, the maximum organic fraction was derived as 13.7 wt%. This yield decreases by 50% when the temperature increases from 550 to 650 °C. Further analysis of the heating value of the organic fraction is presented in section 3.4.4. At 650 °C, secondary cracking reactions contribute to a decrease in the organic fraction, which is reflected by higher yields of gas and water [58].

3.5.2. Gas composition

Fig. 5 shows the yields of the major gas compounds from the bench-scale pyrolysis experiments. Hydrogen sulfide was out of the detection range of the Py-GC/MS with the setup utilized in this study. Nevertheless, the production of hydrogen sulfide gas can be detected in fixed bed experiments though micro-GC. In the experimental temperature range, H_2, CH_4, CO, C_2H_4, and C_3H_8 show strong positive correlations with temperature. The yields of H_2S and C_3H_6 are not sensitive to the temperature within the range 450–650 °C. The production of these gases increased more than 200% from 450 to 650 °C. However, CO_2 presents a weak positive correlation with temperature, which is in accordance with the results of a previous study [42]. The heating value of the gas product

Table 4
The kinetic and thermodynamic parameters obtained in this study and other previous works.

	Materials	Method	Temperature range	Pseudo	Heating rate	E_a/ $E_{a,mean}$	log(A)/ $log(A)_{mean}$	$\Delta H^{\ddagger}/\Delta H^{\ddagger}_{mean}$	$\Delta G^{\ddagger}/\Delta G^{\ddagger}_{mean}$	$\Delta S^{\ddagger}/\Delta S^{\ddagger}_{mean}$
	(°C)				(°C/min)	kJ/mol	s^{-1}	kJ/mol	kJ/mol	J/mol.K
Present work	HPPMS	Friedman	162–594	–	10, 15, 20	233.08	17.83	169.85 –315.60	159.39 –198.87	−48.19 - 235.78
	HPPMS	KAS	162–594	–	10, 15, 20	209.78	15.97	188.91 –260.74	158.59 –191.55	−4.45 - 145.80
	HPPMS	OFW	162–594	–	10, 15, 20	207.46	15.96	189.13 –260.85	159.29 –192.07	−4.96 - 145.32
Yu et al. [48]	Paper sludge	–	<743	–	10	200.32	10.18	–	–	–
	Paper sludge	–	<743	–	15	189.47	9.60	–	–	–
	Paper sludge	–	<743	–	20	231.63	11.98	–	–	–
	Paper sludge	–	<743	–	30	187.26	9.55	–	–	–
Vamvuka et al. [49]	Paper sludge	F1	230–390	Hemicellulose	10	107.1	9.04	–	–	–
	Paper sludge	F1	310–410	Cellulose	10	228.5	18.69	–	–	–
	Paper sludge	F1	200–850	Lignin	10	28.1	0.91	–	–	–
Lin et al. [45]	Paper sludge	Friedman	100–1000	–	20, 30, 40	212	–	–	–	–
	Paper sludge	Starink	100–1000	–	20, 30, 40	217	–	–	–	–
Ma et al. [46]	Hydro-Sawdust	OFW	200–520	–	10, 20, 30, 40	174.01	12.46	168.09	183.32	−23.45
	Hydro-Sawdust	KAS	200–520	–	10, 20, 30, 40	172.64				
	Hydro-Sewage sludge	OFW	140–810	–	10, 20, 30, 40	308.94	46.68	306.77	154.57	270.00
	Hydro-Sewage sludge	KAS	140–810	–	10, 20, 30, 40	314.78				
Rony et al. [50]	Corn stover	OFW	160–700	–	10, 20, 30, 40	191.57	12.62–17.88	162–221	171–172	−16 - 82
	Corn stover	KAS	160–700	–	10, 20, 30, 40	181.66	11.82–16.91	153–210	171–172	−31 - 63.5

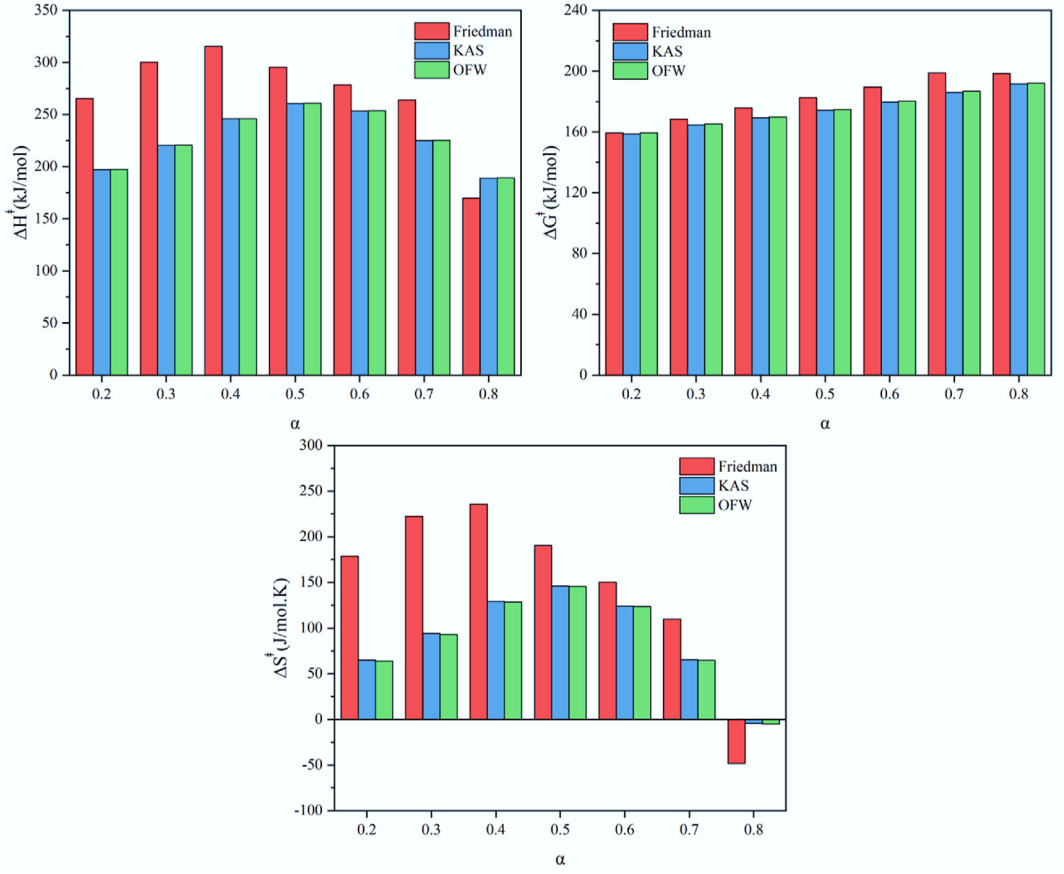

Fig. 3. The $\Delta H^{\ddagger}$, $\Delta H^{\ddagger}G^{\ddagger}$, and $\Delta S^{\ddagger}$ at different conversion degrees of the pyrolysis of HPPMS deduced by using the KAS, OFW, and Friedman methods.

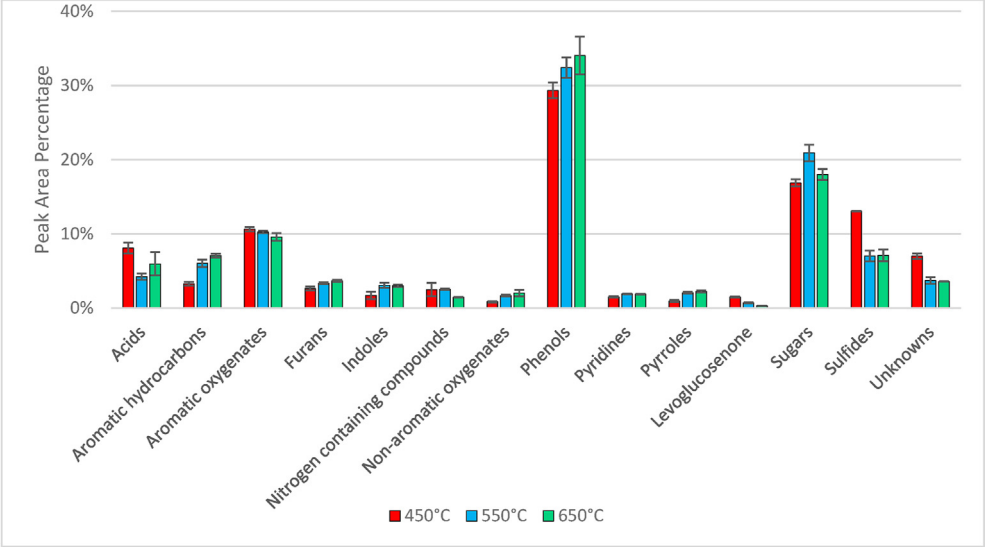

Fig. 4. Peak area percentage of the compound distribution in the pyrolytic vapour of HPPMS in Py-GC/MS.

Table 5
Product distribution results from bench-scale pyrolysis experiments (wt%).

Temperature (°C)	Char	Gas[a]	Organic fraction	Aqueous fraction	Total liquid
450	53.7	16.9	13.6	15.8	29.4
550	49.3	20.4	13.7	16.6	30.3
650	44.9	29.7	6.8	18.6	25.4

[a] Calculated by the difference.

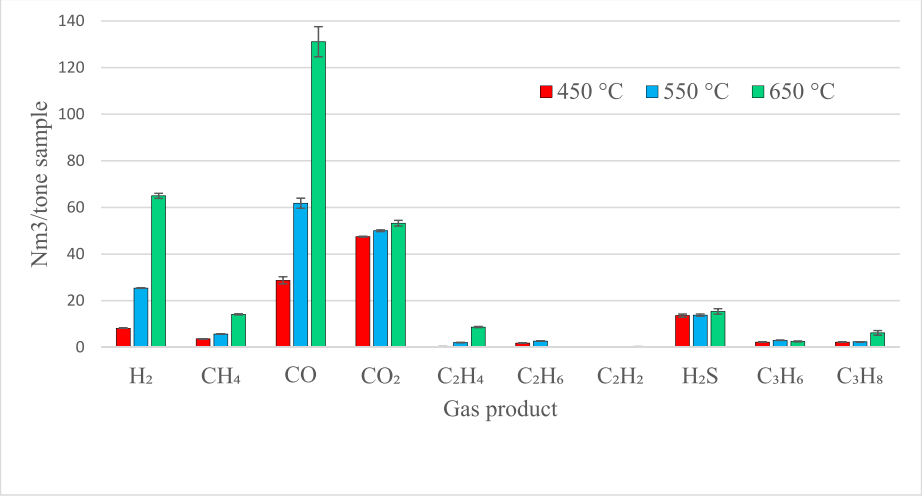

Fig. 5. Gas production from bench-scale pyrolysis experiments.

was calculated and is presented in Table 6. The HHV of gas product increased from 14.1 to 16.3 MJ/Nm^3 when the temperature increase from 450 to 650 °C. The HHV of gas product is much lower than the natural gas (40.6 MJ/Nm^3), because of the high CO_2 content [59]. In order to use the gas product as gaseous fuel, an upgrading process might be required to remove the CO_2.

3.5.3. Analysis of char

The ultimate and proximate results of the char obtained from the bench-scale pyrolysis experiments are presented in Table 7. The ash content and fixed carbon content of char increased with increasing temperature because additional organics decomposed at higher temperatures. In contrast, the volatile matter shows a negative correlation with temperature. The higher heating value (HHV) of char varies from 22.3 to 23.7 MJ/kg, which is close to the HHV of anthracite 30 MJ/kg [59]. The biochar half-life refer to the half-life time of C in the biochar [60,61]. The biochar with a higher half-life indicates a stronger potential on application as carbon sink. Biochar with a molar ratio of O:C less than 0.2 provides a minimum biochar half-life of 1000 years; when the molar ratio is between 0.2 and 0.6, a 100–1000 year biochar half-life is expected; and when it is larger than 0.6, the biochar half-life is usually less than 100 years

Table 6
Gas composition (vol%) and HHV (MJ/Nm^3).

	H_2	CH_4	CO	CO_2	C_2H_4	C_2H_6	C_2H_2	H_2S	C_3H_6	C_3H_8	HHV
450 °C	7.6	3.4	26.6	43.9	0.2	1.6	0.1	12.5	2.1	2.0	14.1
550 °C	15.2	3.4	37.1	30.0	1.2	1.6	0.0	8.3	1.8	1.4	15.0
650 °C	21.9	4.8	44.2	18.0	2.9	0.0	0.1	5.2	0.8	2.1	16.3

Table 7
Ultimate and proximate analysis of char product (wt%).

	450 °C	550 °C	650 °C
Proximate analysis			
Ash content	25.8	29.7	30.7
Volatile matter	33.6	28.2	16.9
Fixed C	40.6	42.1	52.4
O:C ratio	0.09	0.04	0.01
HHV (MJ/kg)	23.0	22.3	23.7
Ultimate analysis (wt%)			
S	0.8	1.1	1.5
Cl	0.03	0.03	0.03
C	59.4	59.9	63.3
H	2.3	1.6	1.1
N	4.5	4.3	3.0
O[a]	7.1	3.4	0.5

[a] Calculated by the difference.

Table 8
Elemental composition, HHV and water content of the organic fraction and aqueous fraction.

	450_o	550_o	650_o	450_a	550_a	650_a
C	71.52	74.02	75.70	9.90	8.70	5.99
H	8.85	8.69	6.69	9.94	10.10	10.2
O[a]	13.51	10.68	10.54	74.95	75.56	77.82
N	5.23	5.59	6.27	5.21	5.64	5.99
S	0.83	1.03	0.80	–	–	–
HHV (MJ/kg)	34.77	35.91	33.61	4.26	3.98	2.80
Water content	–	–	–	72.48	74.48	78.77

[a] Calculated by difference; $_o$: organic fraction; $_a$: aqueous fraction.

[61]. In this study, the O:C ratio decrease when the temperature increase. The molar ratios of O:C of all the char products are less than 0.2, which shows that all of the char has the potential to be a carbon sink in the soil.

The sulfur content in the char increased with increasing temperature. This shows that the state of residual sulfur in the char after pyrolysis is chemically stable until undergoing thermal decomposition at 650 °C. In contrast, the nitrogen and hydrogen content decreased when the temperature increased, which shows that higher temperatures contribute to nitrogen and hydrogen removal from char.

3.5.4. Characterization of liquid

The elemental composition, HHV, and water content of the organic fraction and aqueous fraction (including water) are presented in Table 8. The highest HHV was found with the organic fraction produced from the experiment at 550 °C. From 450 to 550 °C, the carbon content increased by 2.5%, the oxygen content decreased by 2.8%, and the HHV increased from 34.8 to 35.9 MJ/kg, which is the highest heating value of the investigated temperatures. However, the organic fraction yielded at 650 °C shows a lower HHV than the values obtained at temperatures from 450 to 550 °C, which is due to the removal of H and S at high temperature. The water content shows a positive correlation with temperature, resulting in additional cracking reactions at a higher temperature, which would enhance water production.

Research on the pyrolysis of dry PPMS without HTC pretreatment has been investigated in previous studies [62–66]. Ouadi et al. found bio-oil with a calculated heating value of 36–37 MJ/kg (dry basis) in experiments performed on a pyroformer intermediate pyrolysis system at 450 °C [63]. Previous research studied HTC-treated digested municipal sewage sludge pyrolysis on TG, Py-GC/MS and bench-scale reactors from 450 to 650 °C. It was found that only 1.8–3.3 wt% of the feedstock was converted into an organic fraction with higher heating values of 28.47–38.46 MJ/kg [35].

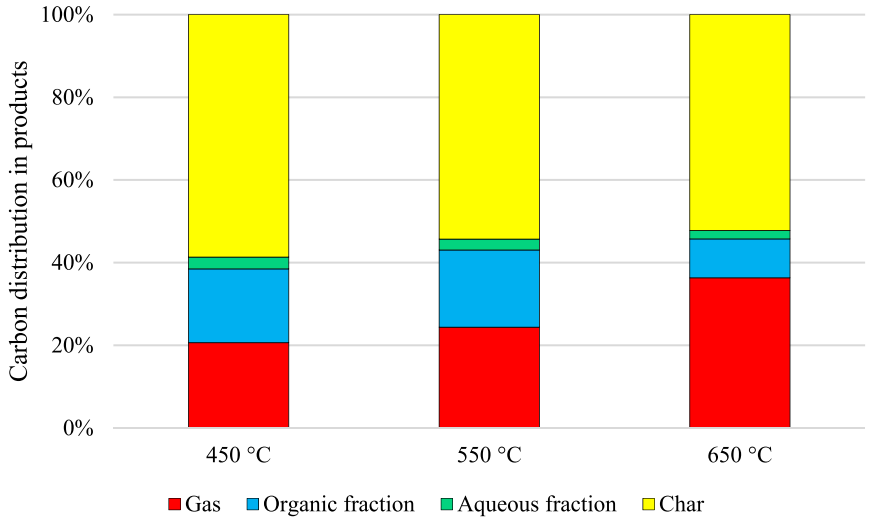

Fig. 6. The carbon distribution in products based on the carbon content of HPPMS.

Table 9
Ratio of energy of product to energy of feedstock.

	Gas	Organic fraction	Aqueous fraction	Char	Energy loss
450 °C	0.08	0.22	0.03	0.57	0.10
550 °C	0.13	0.23	0.02	0.51	0.11
650 °C	0.23	0.11	0.02	0.49	0.15

3.5.5. Carbon distribution and energy balance

The carbon distribution in each pyrolysis product is presented in Fig. 6. The carbon yield in gas products increased with increases pyrolysis temperature due to the enhanced rate of cracking reactions occurring at relatively high temperatures. At 550 °C, the carbon yield of the organic liquid fraction achieved the highest value of 18.7% among the three temperatures compared to 17.8% and 9.4% at 450 and 650 °C, respectively. Based on the HHV of each product, the energy balance of the pyrolysis process was calculated, as shown in Table 9. The energy loss mainly resulted from the heat released during the cooling of the product. The highest energy yield of the organic fraction was found at 550 °C. The gas and char product contained more than 60% of the energy from the feedstocks.

4. Conclusions

This work investigated the pyrolysis behaviour and kinetics of hydrothermal carbonization-treated PPMS.

Thermodynamic data analysis: The mean activation energy of the pyrolysis of HPPMS was found to be 233.08 kJ/mol by using the Friedman method, which is higher than that of the pyrolysis of paper sludge reported in previous works [45,48]. On the other hand, the activation energy, $\Delta H^{\ddagger}$, $\Delta G^{\ddagger}$, and $\Delta S^{\ddagger}$ of the pyrolysis of HPPMS were found to have values between those of the pyrolysis of hydro-sawdust and hydro-sewage sludge reported in a previous study [46].

Py-GC/MS: The appearance of N-containing compounds revealed the existence of protein content in the feedstock. The peak area percentage of MAH was found to show a positive correlation with temperature. The peak area percentage of PAHs shows a negative correlation with the temperature.

Bench-scale experiments: The production of H_2, CH_4, CO, C_2H_4, and C_3H_8 showed a positive correlation with increased peak temperature of pyrolysis. The biochar from all the cases showed an O:C ratio below 0.2, which presents the potential to be applied as a carbon sink. At 550 °C, 13.7 wt% of the HPPMS converted into an organic fraction with an HHV of 35.91 MJ/kg. This also gave the highest carbon yield (18.7%) and energy of the product to the energy of feedstock ratio (0.23) of the organic fraction.

CRediT authorship contribution statement

Shule Wang: conceived of the presented idea, verified the analytical and experimental methods. have done the Py-GC/MS and bench-scale pyrolysis experiment. completed the analytical work. The research results were evaluated by all the co-authors. It was then reviewed and revised by all of the co-authors. **Yuming Wen:** have done the TG experiment. completed the analytical work. The research results were evaluated by all the co-authors. It was then reviewed and revised by all of the co-authors. The primary manuscript was written. **Henry Hammarström:** conceived of the presented idea. verified the analytical and experimental methods. The research results were evaluated by all the co-authors. **Pär Göran Jönsson:** conceived of the presented idea. verified the analytical and experimental methods. The research results were evaluated by all the co-authors. **Weihong Yang:** conceived of the presented idea. verified the analytical and experimental methods. The research results were evaluated by all the co-authors.

Declaration of competing interest

The authors declare that they have no known competing financial interests or personal relationships that could have appeared to influence the work reported in this paper.

Acknowledgement

The authors acknowledge financial support from the FORMAS-Swedish Research Council for Sustainable Development for funding in the frame of the collaborative international consortium (RECOWATDIG) financed under the 2018 Joint call of the WaterWorks2017 ERA-NET Cofund. The authors also greatly acknowledge C-Green AB for the raw materials and information. Cooperation with Envigas AB is highly appreciated. One of the authors, Shule Wang, would also like to acknowledge the Chinese Scholarship Council (CSC) and his girlfriend Q. Hu for the support of this study.

Appendix A. Supplementary data

Supplementary data to this article can be found online at https://doi.org/10.1016/j.renene.2021.06.027.

References

[1] C. Veluchamy, A.S. Kalamdhad, Influence of pretreatment techniques on anaerobic digestion of pulp and paper mill sludge: a review, Bioresour. Technol. 245 (2017) 1206–1219.
[2] J.E. Naicker, R. Govinden, P. Lekha, B. Sithole, Transformation of pulp and paper mill sludge (PPMS) into a glucose-rich hydrolysate using green chemistry: assessing pretreatment methods for enhanced hydrolysis, J. Environ. Manag. 270 (2020) 110914.
[3] I. Haq, P. Mazumder, A.S. Kalamdhad, Recent advances in removal of lignin from paper industry wastewater and its industrial applications-A review, Bioresource Technology, 2020, p. 123636.
[4] A. Mohammadi, M. Sandberg, G. Venkatesh, S. Eskandari, T. Dalgaard, S. Joseph, K. Granström, Environmental analysis of producing biochar and energy recovery from pulp and paper mill biosludge, J. Ind. Ecol. 23 (5) (2019) 1039–1051.
[5] J. Štefelová, V. Slovák, G. Siqueira, R.T. Olsson, P. Tingaut, T. Zimmermann, H. Sehaqui, Drying and pyrolysis of cellulose nanofibers from wood, bacteria, and algae for char application in oil absorption and dye adsorption, ACS Sustain. Chem. Eng. 5 (3) (2017) 2679–2692.
[6] T. Pröll, R.A. Afif, S. Schaffer, C. Pfeifer, Reduced local emissions and long-term carbon storage through pyrolysis of agricultural waste and application of pyrolysis char for soil improvement, Energy Procedia 114 (2017) 6057–6066.
[7] M. Morin, S. Pécate, M. Hémati, Kinetic study of biomass char combustion in a low temperature fluidized bed reactor, Chem. Eng. J. 331 (2018) 265–277.
[8] S. Wang, H. Persson, W. Yang, P.G. Jönsson, Effect of H2 as pyrolytic agent on the product distribution during catalytic fast pyrolysis of biomass using zeolites, Energy Fuel. 32 (8) (2018) 8530–8536.
[9] H. Weldekidan, V. Strezov, G. Town, T. Kan, Production and analysis of fuels and chemicals obtained from rice husk pyrolysis with concentrated solar radiation, Fuel 233 (2018) 396–403.
[10] K. Akubo, M.A. Nahil, P.T. Williams, Pyrolysis-catalytic steam reforming of agricultural biomass wastes and biomass components for production of hydrogen/syngas, J. Energy Inst. 92 (6) (2019) 1987–1996.
[11] A.S. Giwa, F. Chang, H. Xu, X. Zhang, B. Huang, Y. Li, J. Wu, B. Wang, M. Vakili, K. Wang, Pyrolysis of difficult biodegradable fractions and the real syngas biomethanation performance, J. Clean. Prod. 233 (2019) 711–719.
[12] P. Zhao, S. Ge, D. Ma, C. Areeprasert, K. Yoshikawa, Effect of hydrothermal pretreatment on convective drying characteristics of paper sludge, ACS Sustain. Chem. Eng. 2 (4) (2014) 665–671.
[13] K. Kirtania, Chapter 4 - Thermochemical Conversion Processes for Waste Biorefinery, in: T. Bhaskar, A. Pandey, S.V. Mohan, D.-J. Lee, S.K. Khanal (Eds.), Waste Biorefinery, Elsevier2018, pp. 129-156.
[14] L.J.R. Nunes, J.C. De Oliveira Matias, J.P. Da Silva Catalão, Chapter 1 - introduction, in: L.J.R. Nunes, J.C. De Oliveira Matias, J.P. Da Silva Catalão (Eds.), Torrefaction of Biomass for Energy Applications, Academic Press2018, pp. 1-43.
[15] M. Hu, X. Wang, J. Chen, P. Yang, C. Liu, B. Xiao, D. Guo, Kinetic study and syngas production from pyrolysis of forestry waste, Energy Convers. Manag.

135 (2017) 453–462.
[16] Y. Wen, S. Wang, W. Mu, W. Yang, P.G. Jönsson, Pyrolysis performance of peat moss: a simultaneous in-situ thermal analysis and bench-scale experimental study, Fuel 277 (2020) 118173.
[17] Y. Xu, B. Chen, Investigation of thermodynamic parameters in the pyrolysis conversion of biomass and manure to biochars using thermogravimetric analysis, Bioresour. Technol. 146 (2013) 485–493.
[18] X. Ming, F. Xu, Y. Jiang, P. Zong, B. Wang, J. Li, Y. Qiao, Y. Tian, Thermal degradation of food waste by TG-FTIR and Py-GC/MS: pyrolysis behaviors, products, kinetic and thermodynamic analysis, J. Clean. Prod. 244 (2020) 118713.
[19] H. Persson, W. Yang, Catalytic pyrolysis of demineralized lignocellulosic biomass, Fuel 252 (2019) 200–209.
[20] J. Zhao, W. Xiuwen, J. Hu, Q. Liu, D. Shen, R. Xiao, Thermal degradation of softwood lignin and hardwood lignin by TG-FTIR and Py-GC/MS, Polym. Degrad. Stabil. 108 (2014) 133–138.
[21] X. Gu, X. Ma, L. Li, C. Liu, K. Cheng, Z. Li, Pyrolysis of poplar wood sawdust by TG-FTIR and Py–GC/MS, J. Anal. Appl. Pyrol. 102 (2013) 16–23.
[22] Y. Gao, X.-H. Wang, H.-P. Yang, H.-P. Chen, Characterization of products from hydrothermal treatments of cellulose, Energy 42 (1) (2012) 457–465.
[23] Q.-V. Bach, Ø. Skreiberg, Upgrading biomass fuels via wet torrefaction: a review and comparison with dry torrefaction, Renew. Sustain. Energy Rev. 54 (2016) 665–677.
[24] S.R. Naqvi, R. Tariq, Z. Hameed, I. Ali, M. Naqvi, W.-H. Chen, S. Ceylan, H. Rashid, J. Ahmad, S.A. Taqvi, Pyrolysis of high ash sewage sludge: kinetics and thermodynamic analysis using Coats-Redfern method, Renew. Energy 131 (2019) 854–860.
[25] A. Mabuda, N. Mamphweli, E. Meyer, Model free kinetic analysis of biomass/sorbent blends for gasification purposes, Renew. Sustain. Energy Rev. 53 (2016) 1656–1664.
[26] B. Janković, N. Manić, I. Radović, M. Janković, M. Rajačić, Model-free and model-based kinetics of the combustion process of low rank coals with high ash contents using TGA-DTG-DTA-MS and FTIR techniques, Thermochim. Acta 679 (2019) 178337.
[27] Y. Rahib, B. Sarh, S. Bostyn, S. Bonnamy, T. Boushaki, J. Chaoufi, Non-isothermal kinetic analysis of the combustion of argan shell biomass, Mater. Today: Proceedings 24 (2020) 11–16.
[28] S.R. Naqvi, R. Tariq, Z. Hameed, I. Ali, S.A. Taqvi, M. Naqvi, M. Niazi, T. Noor, W. Farooq, Pyrolysis of high-ash sewage sludge: thermo-kinetic study using TGA and artificial neural networks, Fuel 233 (2018) 529–538.
[29] J.H. Flynn, L.A. Wall, General treatment of the thermogravimetry of polymers, J. Resear. Nat. Bureau Stand. Sect. A, Phys. Chem. 70 (6) (1966) 487.
[30] K. Slopiecka, P. Bartocci, F. Fantozzi, Thermogravimetric analysis and kinetic study of poplar wood pyrolysis, Appl. Energy 97 (2012) 491–497.
[31] R.K. Mishra, K. Mohanty, Pyrolysis kinetics and thermal behavior of waste sawdust biomass using thermogravimetric analysis, Bioresour. Technol. 251 (2018) 63–74.
[32] H. Shahbeig, M. Nosrati, Pyrolysis of municipal sewage sludge for bioenergy production: thermo-kinetic studies, evolved gas analysis, and techno-socio-economic assessment, Renew. Sustain. Energy Rev. 119 (2020) 109567.
[33] H. Persson, T. Han, L. Sandström, W. Xia, P. Evangelopoulos, W. Yang, Fractionation of liquid products from pyrolysis of lignocellulosic biomass by stepwise thermal treatment, Energy 154 (2018) 346–351.
[34] H. Persson, I. Duman, S. Wang, L.J. Pettersson, W. Yang, Catalytic pyrolysis over transition metal-modified zeolites: a comparative study between catalyst activity and deactivation, J. Anal. Appl. Pyrol. 138 (2019) 54–61.
[35] S. Wang, H. Persson, W. Yang, P.G. Jönsson, Pyrolysis study of hydrothermal carbonization-treated digested sewage sludge using a Py-GC/MS and a bench-scale pyrolyzer, Fuel (2020) 262.
[36] Engineering ToolBox, Gross and Net Heating Values for Some Common Gases, 2003. https://www.engineeringtoolbox.com/gross-net-heating-values-d_420.html.
[37] J.H. Perry, Chemical engineers' handbook, J. Chem. Educ. 27 (9) (1950) 533.
[38] A. International, ASTM E203-16, Standard Test Method for Water Using Volumetric, Karl Fischer Titration, West Conshohocken, PA, 2016.
[39] P. Axegård, C-Green's HTC-Solution for Conversion of Biosludge to Hydrochar, 2nd International Symposium on Hydrothermal Carbonization Berlin, 2019.
[40] N. Sophonrat, L. Sandström, I.N. Zaini, W. Yang, Stepwise pyrolysis of mixed plastics and paper for separation of oxygenated and hydrocarbon condensates, Appl. Energy 229 (2018) 314–325.
[41] P. Biller, A.B. Ross, 17 - production of biofuels via hydrothermal conversion, in: R. Luque, C.S.K. Lin, K. Wilson, J. Clark (Eds.), Handbook of Biofuels Production (second ed.), Woodhead Publishing2016, pp. 509-547.
[42] Z. Yao, X. Ma, Z. Wu, T. Yao, TGA–FTIR analysis of co-pyrolysis characteristics of hydrochar and paper sludge, J. Anal. Appl. Pyrol. 123 (2017) 40–48.
[43] N. Manić, B. Janković, V. Dodevski, Model-free and model-based kinetic analysis of Poplar fluff (Populus alba) pyrolysis process under dynamic conditions, J. Therm. Anal. Calorim. (2020) 1–20.
[44] S.D. Stefanidis, K.G. Kalogiannis, E.F. Iliopoulou, C.M. Michailof, P.A. Pilavachi, A.A. Lappas, A study of lignocellulosic biomass pyrolysis via the pyrolysis of cellulose, hemicellulose and lignin, J. Anal. Appl. Pyrol. 105 (2014) 143–150.
[45] Y. Lin, X. Ma, Z. Yu, Y. Cao, Investigation on thermochemical behavior of co-pyrolysis between oil-palm solid wastes and paper sludge, Bioresour. Technol. 166 (2014) 444–450.
[46] J. Ma, H. Luo, Y. Li, Z. Liu, D. Li, C. Gai, W. Jiao, Pyrolysis kinetics and thermodynamic parameters of the hydrochars derived from co-hydrothermal carbonization of sawdust and sewage sludge using thermogravimetric analysis, Bioresour. Technol. 282 (2019) 133–141.
[47] R.K. Mishra, K. Mohanty, X. Wang, Pyrolysis kinetic behavior and Py-GC–MS analysis of waste dahlia flowers into renewable fuel and value-added chemicals, Fuel 260 (2020) 116338.
[48] Y.H. Yu, S.D. Kim, J.M. Lee, K.H. Lee, Kinetic studies of dehydration, pyrolysis and combustion of paper sludge, Energy 27 (5) (2002) 457–469.
[49] D. Vamvuka, N. Salpigidou, E. Kastanaki, S. Sfakiotakis, Possibility of using paper sludge in co-firing applications, Fuel 88 (4) (2009) 637–643.
[50] A.H. Rony, L. Kong, W. Lu, M. Dejam, H. Adidharma, K.A. Gasem, Y. Zheng, U. Norton, M. Fan, Kinetics, thermodynamics, and physical characterization of corn stover (Zea mays) for solar biomass pyrolysis potential analysis, Bioresour. Technol. 284 (2019) 466–473.
[51] C.T. Chong, G.R. Mong, J.-H. Ng, W.W.F. Chong, F.N. Ani, S.S. Lam, H.C. Ong, Pyrolysis characteristics and kinetic studies of horse manure using thermogravimetric analysis, Energy Convers. Manag. 180 (2019) 1260–1267.
[52] H. Cao, Y. Xin, D. Wang, Q. Yuan, Pyrolysis characteristics of cattle manures using a discrete distributed activation energy model, Bioresour. Technol. 172 (2014) 219–225.
[53] R. Kaur, P. Gera, M.K. Jha, T. Bhaskar, Pyrolysis kinetics and thermodynamic parameters of castor (Ricinus communis) residue using thermogravimetric analysis, Bioresour. Technol. 250 (2018) 422–428.
[54] Q. Wang, H. Song, S. Pan, N. Dong, X. Wang, S. Sun, Initial pyrolysis mechanism and product formation of cellulose: an Experimental and Density functional theory(DFT) study, Sci. Rep. 10 (1) (2020) 3626.
[55] Z. Gao, N. Li, M. Chen, W. Yi, Comparative study on the pyrolysis of cellulose and its model compounds, Fuel Process. Technol. 193 (2019) 131–140.
[56] L. Leng, L. Yang, J. Chen, S. Leng, H. Li, H. Li, X. Yuan, W. Zhou, H. Huang, A review on pyrolysis of protein-rich biomass: nitrogen transformation, Bioresour. Technol. 315 (2020) 123801.
[57] T. Liu, Y. Guo, N. Peng, Q. Lang, Y. Xia, C. Gai, Q. Zheng, Z. Liu, Identification and quantification of polycyclic aromatic hydrocarbons generated during pyrolysis of sewage sludge: effect of hydrothermal carbonization pretreatment, J. Anal. Appl. Pyrol. 130 (2018) 99–105.
[58] C. Liu, H. Wang, A.M. Karim, J. Sun, Y. Wang, Catalytic fast pyrolysis of lignocellulosic biomass, Chem. Soc. Rev. 43 (22) (2014) 7594–7623.
[59] Standard Grade Coal - Heat Value, 2021. https://www.engineeringtoolbox.com/coal-heating-values-d_1675.html. (Accessed 17 May 2021).
[60] C.-C. Tsai, Y.-F. Chang, Kinetics of C Mineralization of biochars in three excessive compost-fertilized soils: effects of feedstocks and soil properties, Agronomy 10 (11) (2020).
[61] K.A. Spokas, Review of the stability of biochar in soils: predictability of O:C molar ratios, Carbon Manag. 1 (2) (2010) 289–303.
[62] R. Lou, S. Wu, G. Lv, Q. Yang, Energy and resource utilization of deinking sludge pyrolysis, Appl. Energy 90 (1) (2012) 46–50.
[63] M. Ouadi, J.G. Brammer, Y. Yang, A. Hornung, M. Kay, The intermediate pyrolysis of de-inking sludge to produce a sustainable liquid fuel, J. Anal. Appl. Pyrol. 102 (2013) 24–32.
[64] J. Jiang, X. Ma, Experimental research of microwave pyrolysis about paper mill sludge, Appl. Therm. Eng. 31 (17–18) (2011) 3897–3903.
[65] V. Strezov, T.J. Evans, Thermal processing of paper sludge and characterisation of its pyrolysis products, Waste Manag. 29 (5) (2009) 1644–1648.
[66] A.J. Ridout, M. Carrier, F.-X. Collard, J. Görgens, Energy conversion assessment of vacuum, slow and fast pyrolysis processes for low and high ash paper waste sludge, Energy Convers. Manag. 111 (2016) 103–114.